Research

Extraction and purification of malaria vaccine candidate CLCT produced by transient expression in *Nicotiana benthamiana* plants

Matthias Knödler[1,2] · **Johannes F. Buyel[1,3]**

Abstract

Plasmodium falciparum is a malaria parasite that infects more than 220 million people every year. Various non-vaccine campaigns have failed to eradicate malaria and the World Health Organization has recommended only a single malaria vaccine, but this has mediocre efficacy. Additional efforts are therefore required to design and produce medicines that trigger a highly protective immune response. Importantly, the production of such medicines must be cost-efficient to ensure availability in developing countries of the global south, especially sub-Saharan Africa, where they are most needed. Here, we report the development of downstream processing for the novel malaria vaccine candidate CLCT. This fusion protein combines four *P. falciparum* antigens and was produced by transient expression in *Nicotiana benthamiana* plants using *Rhizobium radiobacter* (formerly *Agrobacterium tumefaciens*). The protein accumulated to levels of 118.8 mg kg^{-1} and the blanching of plant biomass enabled the efficient precipitation of > 90% of host cell proteins, thereby achieving a ~ 25-fold increase in the purity of the heat-stable target protein in the homogenate. Plant extracts were clarified by a series of bag, depth and sterile filtration steps with an overall recovery of 36.6%. An ultrafiltration/diafiltration step was then used for buffer exchange and to concentrate the product 2.6-fold, with a step recovery of ~ 65%. We optimized a hydrophobic interaction chromatography capture step, achieving a CLCT recovery of ~ 40%. The overall process yield of purified CLCT was ~ 12 mg kg^{-1} biomass with a final purity of ~ 83%, which is sufficient for initial activity testing in preclinical animal model immunization studies.

Keywords Biopharmaceutical manufacturing · Bioprocess engineering · Downstream process development · Optimized chromatographic separation · Plant molecular farming

Abbreviations
CV   Column volume
DSP   Downstream processing
FF   Fast flow
FT   Flow through
HCP   Host cell protein
HTS   High-throughput screening

HIC   Hydrophobic interaction chromatography
MMCO   Molecular mass cut off
TSP   Total soluble protein
UF/DF   Ultrafiltration/diafiltration

1 Introduction

Malaria is a life-threatening disease caused by parasites of the genus *Plasmodium*, which are transmitted into the subcutaneous tissues of human hosts via infected female mosquitos (genus *Anopheles*) during a blood meal [1, 2]. There are > 400 different *Anopheles* species [1] and *P. falciparum* is the most virulent malaria parasite, accounting for ~ 80% of all infections and ~ 90% of malaria-related deaths, mainly in children [2]. Infection leads to an acute febrile illness featuring headaches and chills, with the first symptoms appearing after 10–15 days [1]. Without treatment, *P. falciparum* malaria can progress to severe illness and 0.3–2.2% of such cases are fatal [1, 3–5]. Between 2010 and 2015, the incidence of malaria fell by 21% and the mortality rate by 29%, but the World Health Organization (WHO) estimates that ~ 212 million people are infected worldwide [6].

The transmission of malaria can be prevented by mechanical vector control, chemoprevention, or potentially by vaccination [6]. However, there is widespread resistance to anti-malaria medicines such as chloroquine and sulfadoxine-pyrimethamine, and resistance is also emerging against artemisinin, which is a component of the WHO malaria control measures and is used for artemisinin combination therapy [1]. The most recent 80 + vaccine candidates (Table S1), including RTS,S/AS01E (currently undergoing phase IV clinical testing, NCT02251704) have achieved limited success in preventing malaria infection and transmission, with an efficacy of 25–78% [6–16]. Such vaccines can target different stages of the complex pathogen life cycle (Fig. 1) by providing the corresponding antigens. For example, circumsporozoite protein (CSP) is present during the pre-erythrocytic stage and is included in RTS,S/AS01E to prevent infection, whereas *Pf*AMA1 is present during the blood stage and is included to prevent clinical manifestation [7, 17]. So-called transmission blocking vaccines are based on sexual-stage antigens to prevent vector-based transmission.

Combining key antigens from different stages of the *P. falciparum* life cycle in a single polyvalent/multi-epitope construct could create an efficient multi-stage malaria vaccine that could prevent infection, clinical manifestation and transmission [7, 12]. In addition, multi-epitope constructs can simplify manufacturing compared to a set of individual proteins [12], but they reduce the flexibility of vaccine composition in terms of epitopes [7]. In this context, a novel malaria vaccine candidate known as CLCT was constructed as a derivative of the previously described CCT [19, 23] and contains *P. falciparum* epitopes of cell traversal protein from ookinetes and sporozoites (CelTOS), CSP, thrombospondin-related adhesive protein (TRAP) and a C-terminal tandem repeat of 18× NANP (single letter amino acid code) which is found in CSP [7, 19, 24, 25]. These sequences represent important pre-erythrocytic antigens within the *P. falciparum* life cycle and have been used individually in other vaccine candidates currently undergoing clinical trials (Table S1). Combining the antigens to a poly-antigen fusion protein can reduce the overall production effort while providing multiple epitopes for efficient immunization in a single molecule. The protein was produced in *Nicotiana benthamiana* by infiltration with *Rhizobium radiobacter* (formerly *Agrobacterium tumefaciens*) because transient expression in plants facilitates the rapid and low-cost manufacturing of complex proteins and can be scaled-up massively, for example in fully controlled vertical farming units (VFUs) [22, 26–30]. However, downstream processing (DSP) can be challenging due to the presence of abundant particles and host cell proteins (HCPs) [31]. Therefore, this study focused on the manufacturability of the protein. Specifically, we reduced the quantity of soluble HCPs in the plant biomass by introducing a blanching step [32] before extracting CLCT from the plants. The extract was then clarified in a series of filtration steps and concentrated by ultrafiltration/diafiltration (UF/DF) before purification of the CLCT protein using an optimized hydrophobic interaction chromatography (HIC) step (Fig. 2).

2 Materials and methods

2.1 Expression vectors and bacterial strains

Rhizobium radiobacter strain GV3101::pMP90RK carrying the expression vector pTRAkc-CLCT-SEKDEL encoding CLCT targeted to the endoplasmic reticulum (ER) (Fig. 1F, G), was used for transient expression of CLCT (Fig. 1H, I) in *N. benthamiana*.

2.2 Cultivation of R. radiobacter

We cultivated *R. radiobacter* at 27 °C for 3 days on a shaker at 160 rpm (25 mm eccentricity). We inoculated 50 mL of plant peptone *Agrobacterium* medium (PAM4) [33, 34] in a 200-mL Schott flak (Schott, Mainz, Germany) with 200 µL of *R. radiobacter* glycerol stock solution (OD_{600nm} = 1.0) to obtain a pre-culture. Before inoculation, we added kanamycin (25 mg L^{-1}), rifampicin (25 mg L^{-1}) and carbenicillin (50 mg L^{-1}) to the PAM4 medium. Infiltration experiments used 50 mL of pre-culture to inoculate three 0.5-L aliquots of PAM4 in 2.0-L Schott flasks containing the same antibiotics as above. The main culture was grown at 27 °C for 3 days on a shaker at 160 rpm. Before infiltration, the bacterial cultures were diluted with 2× infiltration-medium and tap water to a final OD_{600nm} of 1.0. The freshly prepared infiltration solution was used for the infiltration of *N. benthamiana* [36].

2.3 Cultivation of *N. benthamiana*

Nicotiana benthamiana seeds were germinated in stone wool blocks (Cultilene, Tilburg, Netherlands) and were cultivated hydroponically in a phytotron in 0.12 m wide polypropylene gullies ~ 4 m in length at 70% relative humidity and 25/22°C day/night temperature with a 16-h photoperiod provided by GreenPower DR/B 120 LEDs (Phillips, Amsterdam, Netherlands). The light intensity was 140 µmol s^{-1} m^{-2} at the stone wool surface. Automated periodic watering was carried out using the nutrient film technique (NFT), involving 5 min h^{-1} flow at a flow rate of ~ 0.75 L min^{-1} in each gully. Ferty 2 MEGA plant fertilizer (Plantafert, Regenstauf, Germany) with a conductivity of 1.2 mS cm^{-1} (~ 0.8 g L^{-1}) was used during the first two weeks. The conductivity was increased to 1.4 mS cm^{-1} (weeks 3 and 4), and 1.6 mS cm^{-1} (weeks 5–7), prior to infiltration [35]. *N. benthamiana* plants were grown for 49 days prior to infiltration with *R. radiobacter* suspensions.

2.4 Infiltration of *N. benthamiana* plants

Prior to infiltration, *N. benthamiana* plants grown in stone wool blocks were watered with tap water and incubated for 1 h. Proliferating and old leaves were manually removed. We then carefully immersed inverted *N. benthamiana* plants into a 5-L bucket filled with the infiltration suspension with an OD_{600nm} of 0.5. The setup was placed in a vacuum desiccator. A vacuum of 0.01 MPa was created for 60 s using a suitable pump (Elektro-Wärme-Aachen, Aachen, Germany) and then rapidly released. Infiltrated *N. benthamiana* plants were surface-dried by gentle shaking. The subsequent incubation was carried out upside down for 5 days at 25 °C, 70% relative humidity, and a 16-h photoperiod with a photosynthetic photon flux density (PPFD) of 95 µmol s^{-1} m^{-2} and a yield photon flux density (YPDF) of 79 µmol s^{-1} m^{-2} [36] provided by 8× Osram Lumilux 58 W/830 warm white and 8× Osram 58 W/840 cool white lights (Osram, Munich, Germany). The plants were watered with tap water 1 and 3 days post-infiltration (dpi). After 5 days, infiltrated *N. benthamiana* leaves were harvested and used for blanching or extraction [37].

2.5 Blanching of plant biomass

Leaves were harvested 5 dpi and were submerged into a stainless-steel vessel (Clatronic, Kempen, Germany) containing 20 L of heated blanching buffer (40 mM disodium phosphate, pH 8.0) at 80 °C for 10 min. The blanching buffer was agitated continuously using an external MD-6Z magnet pump (Iwaki, Willich, Germany). The leaves were then immersed in water at ~ 15 °C for 1 min before storage at − 20 °C or immediate extraction.

2.6 Extraction of plant biomass

Target proteins were extracted from freshly harvested, frozen or blanched *N. benthamiana* plant material. We added 3 mL of extraction buffer per gram biomass before homogenizing leaves using a blender (Waring, Stamford, USA) three times for 30 s with 30-s pauses. The conductivity, turbidity and pH of the resulting homogenate were measured. A 0.4 M trisodium phosphate solution was used to immediately adjusted the homogenate to pH 8.0. The turbidity was measured using a 2100P ISO Hach turbidimeter (Hach, Loveland, CO, USA) and a 20-fold dilution of the homogenate to reach a value below 1000 nephelometric turbidity units (NTU). Coarse particles > 10 µm were removed from the homogenate by passage through a BP-410 bag filter (Fuhr, Klein-Winternheim, Germany) with a nominal pore size of 1 µm and a filter area of

Fig. 1 The complex life cycle of *Plasmodium falciparum*. **A** The sporozoite form of the pathogen migrates to the liver after entering the ▶ human blood stream [2]. **B** The sporozoites then actively invade hepatocytes using a transmembrane link between the parasite cytoskeleton and the host cell [18, 19]. During this process, the conserved *Plasmodium* thrombospondin-related anonymous protein (TRAP) links to the pathogen's actin filaments via its cytoplasmic tail while binding to hepatocyte surface proteins via the extracellular portion [18]. TRAP is supported by the circumsporozoite protein (CSP), which binds to heparin sulfate proteoglycans and activates pathogen signaling events promoting cell invasion [20]. Another highly conserved protein required for liver invasion is cell traversal protein for ookinetes and sporozoites (CelTOS) [21]. **C** Red blood cells are invaded by parasites released from ruptured liver cells during the blood stage. **D** The formation of gametocytes represents the initiation of the sexual stage, followed by **E** parasite transmission via mosquitoes. Figure reproduced and modified with permission [22]. Vector maps of plasmids used for the transient expression of CLCT in *Nicotiana benthamiana*: **F** CLCT vector map (pTRAkc-CLCT-SEKDEL). The product of the vector contains an N-terminal leader peptide (LPH) and a C-terminal tag (SEKDEL) for retention in the endoplasmic reticulum. The vector also includes the left border (LB) and right border (RB) flanking the TDNA, which contains the CLCT gene, the cauliflower mosaic virus (CaMV) 35 S promoter and duplicated enhancer (P35SS), the CaMV 35 S polyadenylation signal (pA35S), and scaffold attachment regions (SARs). Furthermore, the vector contains the β-lactamase (*bla*) gene for ampicillin/carbenicillin resistance as well as the *E. coli* ColE1 and *R. radiobacter* RK2 origins of replication (ori). **G** The linear CLCT construct consisting of *Pf*CelTOS (green), *Pf*CSP-NANP, (blue) *Pf*CSP-TSR (orange) and *Pf*TRAP-TSR (cyan) with a size of 1221 base pairs (bps) and the corresponding 3D protein homology models of CLCT generated with I-Tasser (**H**) or Alpha Fold (**I**). The SEKDEL retention tag is shown in yellow. Homology modeling was performed using the protein structure and function prediction online tool I-TASSER or Alpha Fold

0.06 m^2 [38]. A depth filter combining K900P and V100P filter layers with nominal retention ratings of 8–20 and 1–3 µm, respectively, and a filter area of 56 cm^2 each was mounted into a VelaPad 90 filter housing (Pall, Port Washington, USA) and pre-wetted with ~ 200 mL extraction buffer. A constant volumetric flux of 12 mL min^{-1} was applied during depth filtration using a Masterflex SE peristaltic pump (Masterflex, Gelsenkirchen, Germany). The filtration was terminated once the backpressure reached 0.2 MPa. The depth filtrate was then passed through a Sartopore2 150 sterile filter (Sartorius, Göttingen, Germany) with a filter area of 0.015 m^2 and a pore size combination of 0.45 µm and 0.2 µm. Alternatively, a hydrophilic 0.2-µm MiniSart sterile filter syringe (Sartorius) was used for depth filtrate volumes < 0.2 L [36].

2.7 Ultrafiltration/diafiltration

UF/DF was performed using a SartoFlow Slice 200 benchtop crossflow system (Sartorius) combined with membrane cassettes (Sartocon Slice 200 Hydrosart, Sartorius) with nominal molecular mass cutoff (MMCO) values of 30 or 100 kDa. The UF/DF system was operated at a constant transmembrane pressure (TMP) of 0.05 MPa for buffer exchange experiments and 0.1 MPa during membrane sanitization. Buffer exchange was achieved by using a four-fold concentration of the initial sample volume (~ 800 mL) and adding ~ 600 mL of the desired buffer. Buffer exchange steps were repeated until the desired conductivity, pH or UV$_{280nm}$ signal was achieved.

2.8 Small-scale buffer exchange

Buffer exchange of protein samples in volumes < 10 mL was carried out using a HiPrep 26/10 Sephadex G-25 column (Cytiva, Little Chalfont, UK) with a column volume (CV) of 53 mL mounted on an Äkta pure chromatography system (Cytiva). Proteins were injected using a 10-mL Superloop (Cytiva) at a flow rate of 10 mL min^{-1}. A build-in fractionator was used to collect peak samples of the proteins based on the UV$_{280nm}$ signal [36].

2.9 Chromatography resin screening

A JANUS G3 liquid handling station (PerkinElmer, Waltham, MA, USA) was equipped with prepacked 0.2-mL RoboColumns (Repligen, Waltham, MA, USA) for small-scale high-throughput screening (HTS) of various HIC resin types. After equilibration for 10 CV, the columns were loaded with 10 CV of clarified plant extracts followed by a 10 CV washing step and elution in 10 CV of elution buffer. During all steps, the flow rate was kept constant at 8.3×10^{-5} m s^{-1} (0.1 mL min^{-1}). We collected 2.0-mL flow through, wash and elution fractions in deep-well plates for immediate analysis.
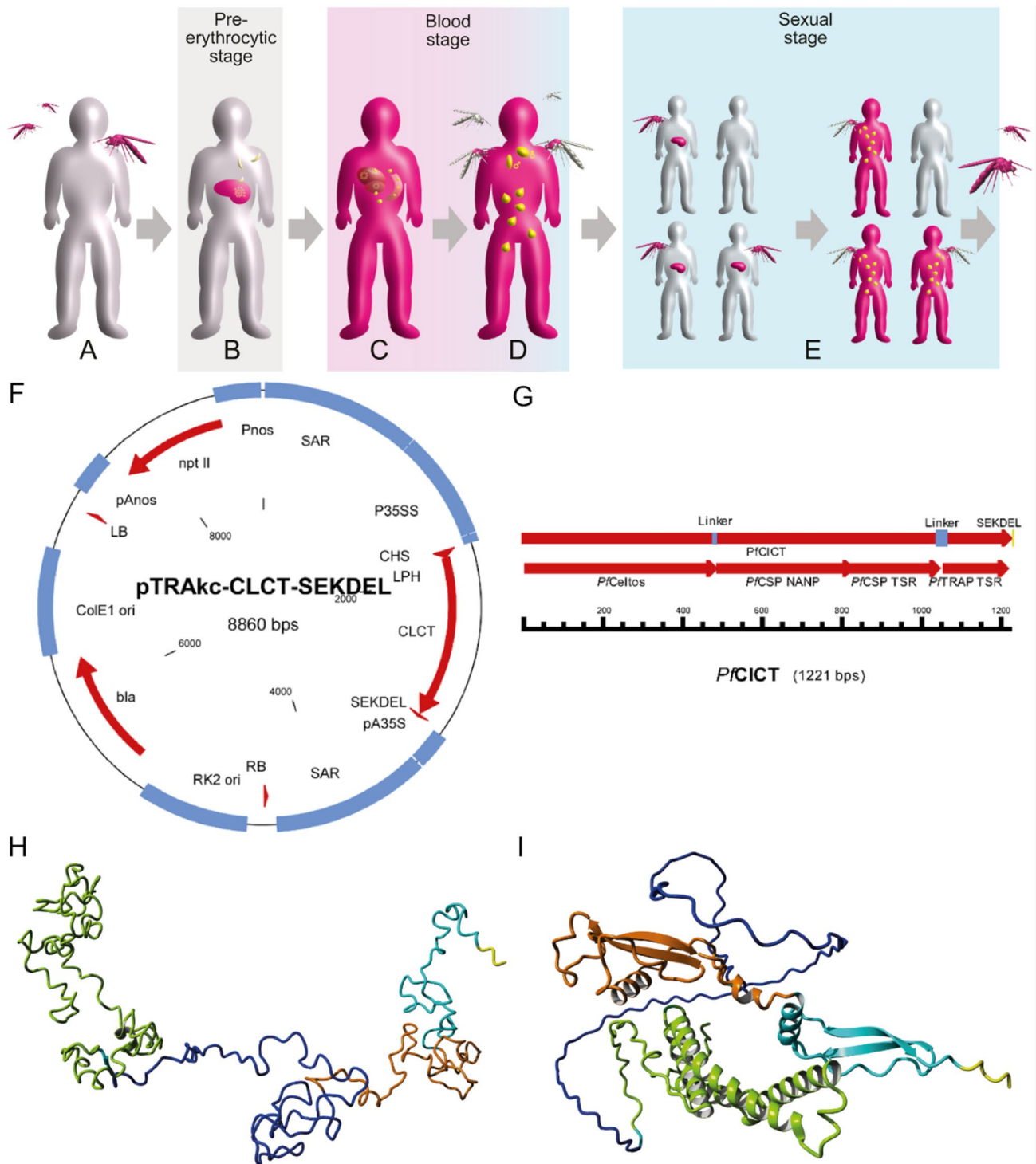
2.10 LDS-PAGE and staining with Coomassie Brilliant Blue

NuPAGE 4–12% Bis-Tris LDS-PAGE gels (Thermo Fisher Scientific, Waltham, MA, USA) with 10, 12, 15 or 26 gel slots were used according to the manufacturer's instructions. Samples containing 1× reducing agent (Thermo Fisher Scientific) and 1x LDS loading buffer (Thermo Fisher Scientific) were denatured for 10 min at 70 °C on a Techne shaking Dri-Block DB-3 heat block (Bibby Scientific, Stone, UK) or alternatively on a Biometra-TRIO PCR cycler (Biometra, Göttingen, Germany). Samples containing salt concentrations ≥ 2 M sodium chloride were heated for another ~ 30 s before loading onto the

gels to avoid phase separation of the protein and buffer. Volumes of 10 µL sample solution or 5 µL 10–180 kDa PageRuler pre-stained protein standard (Thermo Fisher Scientific) were loaded per gel slot. Electrophoresis was carried out in a PowerPac HC electrophoresis module (Bio-Rad Laboratories, Hercules, CA, USA) at 200 V for 37 min. After a 15-min wash with water, gels were stained with SimplyBlue SafeStain (Thermo Fisher Scientific) for 1 h at 22 °C on a rocker (Bibby Scientific, Stone, UK) at 19 rpm. Gels were de-stained in water for 1–2 h and then transferred onto plastic foil for scanning in a CanoScan 5600 F (Canon, Tokyo, Japan). Adobe Photoshop CS5.1 (Adobe, San Jose, CA, USA) at 600 dots per inch was used for image acquisition [36].

2.11 Immunoblotting

Immunoblotting and dot blotting were carried out as described elsewhere [35]. Antibodies used for immunodetection are listed in Table 1.

2.12 Bradford assay

The concentration of total soluble protein (TSP) in 2.5-µL samples was determined according to Bradford [39] using transparent 96-well flat-bottom microplates (Greiner Bio One, Kremsmuenster, Austria). We used 5.0-µL bovine serum albumin (BSA) standards of 2000, 1500, 1000, 750, 500, 250, 125 and 0 mg L^{-1}. After adding 195 µL of Coomassie Protein Assay reagent (Thermo Fisher Scientific) to each well, we mixed the sample and incubated for 10 min at 22 °C. Absorbance was measured twice using an EnSpire multimode plate reader (Perkin Elmer). Protein samples and standards were analyzed in triplicate. Data were exported and analyzed using EnSpire Manager v4.13 (Perkin Elmer).

2.13 Design of experiments

An I-optimal response surface design was set up and analyzed with Design-Expert v12 (Stat-Ease, Minneapolis, MN, USA) to optimize the HIC capture step. The design consisted of 27 runs in five blocks using recovery and purity as responses. More information about the DoE approach can be found elsewhere [40].

3 Results and discussion

3.1 Transient expression of CLCT

The *R. radiobacter* pre-culture and main culture transformed with pTRAkc-CLCT-ERH reached an OD_{600nm} of 6–9 within 2 days. *N. benthamiana* plants were harvested 5 dpi and achieved a biomass of 93.41 ± 12.99 g (± SD, n = 8) per plant. The yield of ER-targeted CLCT was 118.8 ± 20.4 mg kg^{-1} (± SD, n = 3). This was similar to vaccine candidate C9S, which also contains the *Pf*CSP, *Pf*TRAP and *Pf*CelTOS antigens (92.2 ± 6.1 mg kg^{-1}; ± SD, n = 11), and higher than vaccine candidate FQS (48.9 ± 7.8 mg kg^{-1}; ± SD, n = 2) [22, 41]. Product integrity was confirmed by immunoblotting (Fig. 3C,D) using the mouse-derived monoclonal primary antibody α-CSP-TSR (Fraunhofer IME, Aachen, Germany) as a probe. In addition to the expected 44.5-kDa CLCT band, we detected an additional band at ~ 55 kDa, possibly representing a glycosylated variant (Fig. 2C). Whereas there were no *N*-linked glycosylation sites present in the CLCT sequence, the protein contained 39 serine and 12 threonine amino acids that could be subject to *O*-linked glycosylation. Proteins expressed in plants, with molecular masses 2–5 kDa higher than anticipated based on the same protein expressed in other hosts, have been described for many plant-made biopharmaceuticals [42], supporting the presence of plant-specific post-translational modifications [43, 44]. Densitometric analysis of homogenate samples following LDS-PAGE revealed initial purities < 3% of TSP for the 55-kDa product (n = 3, Fig. 2C), highlighting the need for further purification.

3.2 Blanching of plant biomass

Blanching of infiltrated *N. benthamiana* plants increased their mass by 29.02 ± 7.37% (± SD, n = 3) due to the blanching buffer penetrating intercellular spaces and residual blanching buffer on the leaf surface [32, 45]. We accounted

for this higher mass in all subsequent mass balances. Blanching for 2 min also removed > 85% of HCPs, thereby increasing product purity ~ 25-fold without a noticeable drop in product recovery (Fig. 3C, D). This surpassed the 7–14fold increase in purity previously reported for blanching [22, 32]. Although prolonged blanching (2–10 min) did not change the product or HCP concentrations, it improved product stability from 4% to ~ 100% in samples stored for 24 h at 4 °C. We propose that long blanching times probably inactivate some residual proteases, as previously reported [22, 41]. Overall, the results confirmed that blanching is a convenient and straightforward method to simplify DSP for heat-stable target proteins, especially when affinity-based purification methods are unavailable [22, 32, 46].

Fig. 2 Process schematic for the transient expression and purification of the malaria vaccine candidate CLCT produced in *Nicotiana benthamiana* plants. **A** Preparation of *Rhizobium radiobacter* cultures carrying the expression vectors needed for CLCT production in plants. **B** Upstream production of *N. benthamiana* plants followed by infiltration with bacteria. **C** Downstream processing based on a combination of blanching, extraction, filtration, ultrafiltration/diafiltration and optimized hydrophobic interaction chromatography
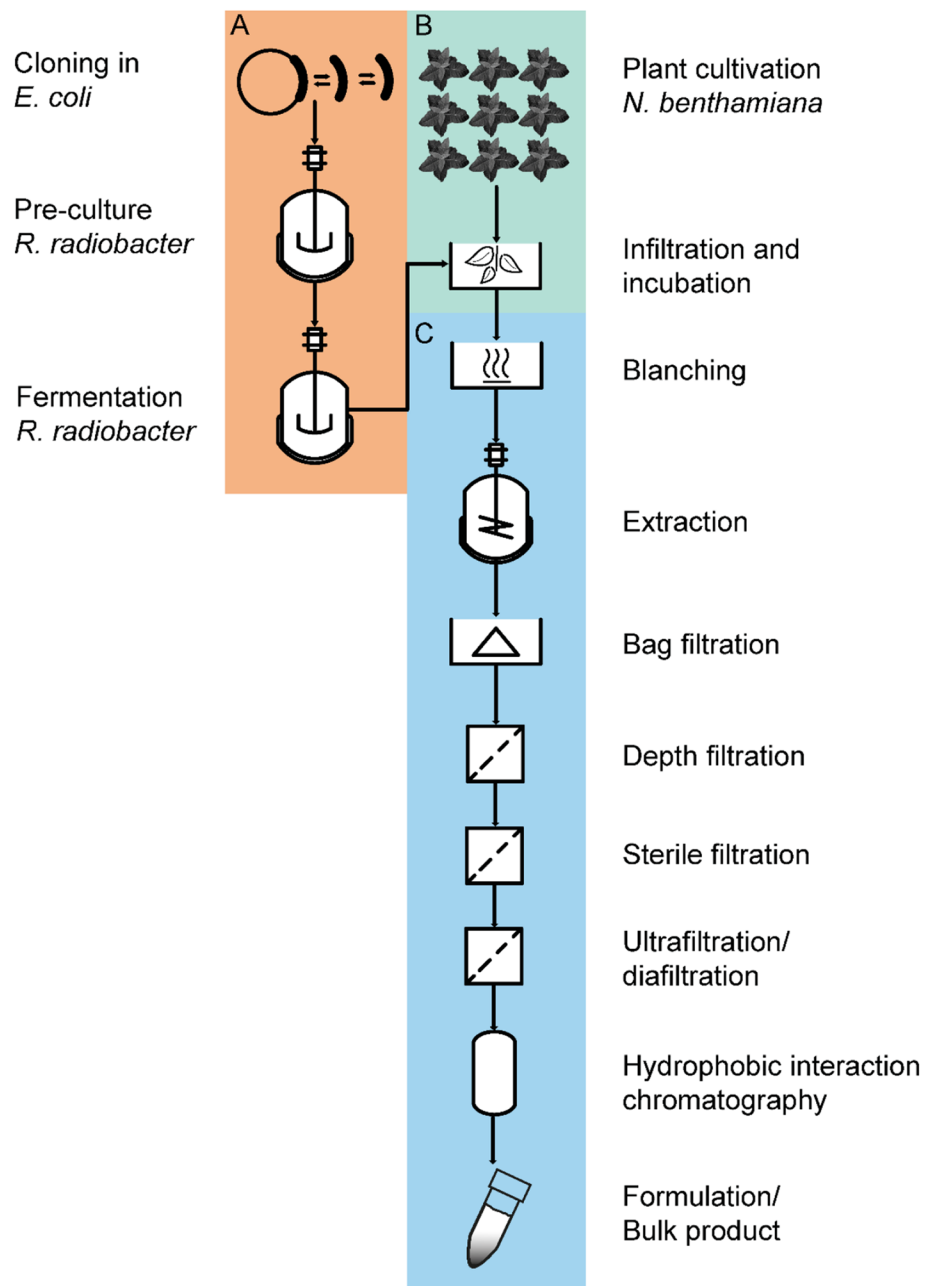
Table 1 Primary and secondary antibodies used for immunodetection

Antibody	Abbreviation	Conjugate	Manufacturer	Used dilution	Concentration
Mouse anti-*Pf*CSP-TSR	–	None	Fraunhofer IME Aachen	1:5000 (v v^{-1})	1.1 [g L^{-1}]
Goat anti-mouse AP	GAM	AP	Jackson	1:5000 (v v^{-1})	0.8 [g L^{-1}]

AP alkaline phosphatase; *Pf*CSP *Plasmodium falciparum* circumsporozoite protein; *TSR* Thrombospondin type 1 repeat domain; *IME* Fraunhofer Institute for Molecular Biology and Applied Ecology IME Aachen, Germany.

3.3 Extraction and clarification

The homogenized plant material was processed by bag filtration, depth filtration and sterile filtration. Product recovery during bag filtration was $97 \pm 2\%$ ($\pm$ SD, n = 3) but the subsequent depth filtration step resulted in a step recovery of only $52 \pm 7\%$ ($\pm$ SD, n = 3) (Fig. 3B). Target proteins can interact with the diatomaceous earth used in depth filters (e.g., the depth filter layer K900P), resulting in lower product recoveries [41, 47]. The filtration capacity of the depth filter layer combination K900P and V100P was 28.5 ± 16.3 L m^{-2} ($\pm$ SD, n = 6) which was slightly lower compared to the untreated plant material (~ 30 L m^{-2}) as previously shown [48]. Countermeasures such as flocculants can help to restore or even improve filter performance [22, 32]. In general, product loss can be reduced during depth filtration if diatomaceous earth is omitted from the filters [38], but this measure did not improve the
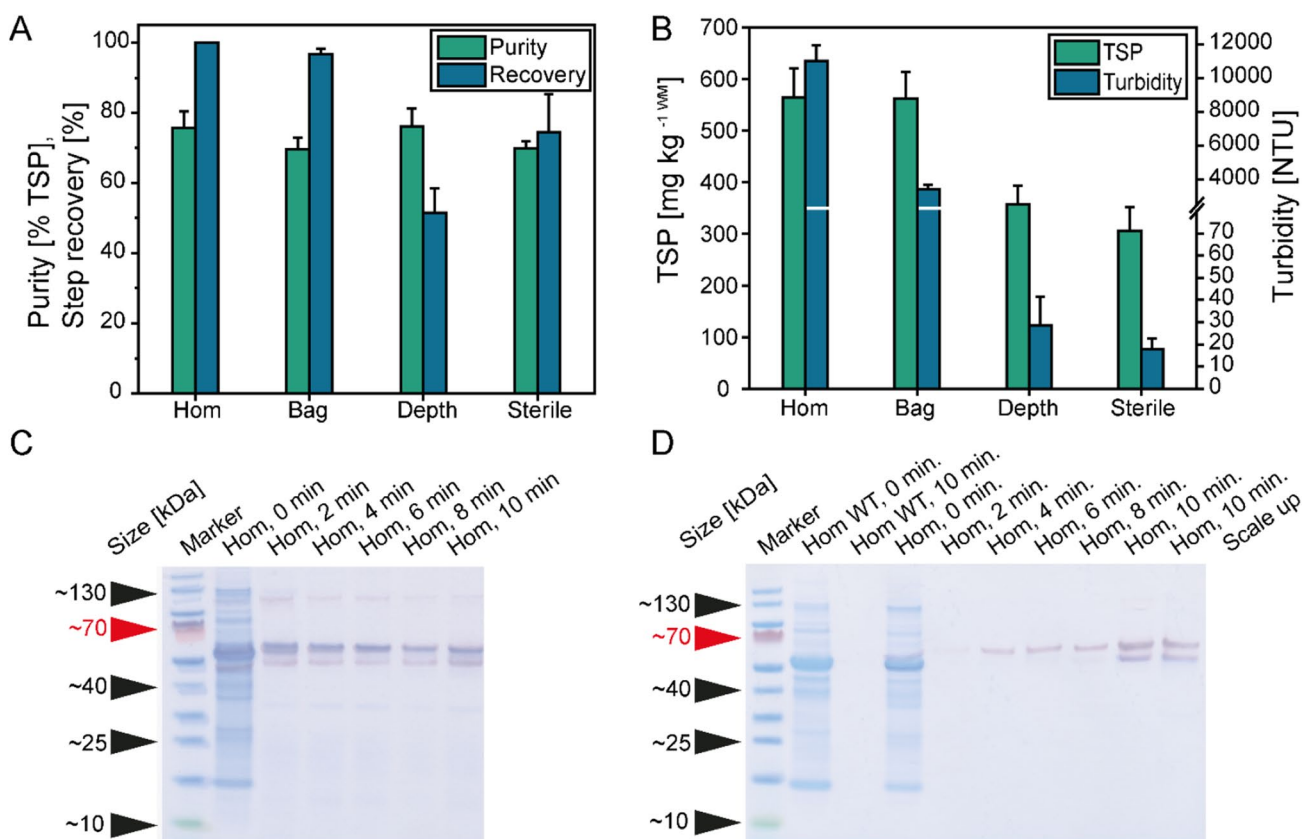

Fig. 3 Transient expression of CLCT and product isolation. **A** Purity and step recovery of CLCT (n ≥ 8) for the different clarification steps: Hom – homogenate, Bag – bag filtrate, Depth – depth filtrate, Sterile – sterile filtrate. **B** Total soluble protein and turbidity of plant extracts from blanched and untreated plants. **C, D** Overlays of stained gels and immunoblots of *N. benthamiana* extracts sampled during heat treatment and analyzed (C) directly after blanching or (**D**) after storage for 24 h, including additional wild-type controls. Marker – PageRuler pre-stained protein ladder (10–177 kDa), WT – wild-type *N. benthamiana*, non-infiltrated. Immunoblots of CLCT were probed using a mouse primary monoclonal antibody against *Pf*CSP-TSR (Table 1) and an AP-conjugated goat anti-mouse (GAM^{AP}) secondary antibody. NTU – nephelometric turbidity units, WM – wet mass

recovery of CLCT (Figure S1). Sterile filtration achieved a step recovery of 74 ± 11% (± SD, n = 3), indicating that the target protein also interacted with the filter membrane. The total recovery after sterile filtration was 37 ± 1% (± SD, n = 3), which is comparable to a similar purification process applied to vaccine candidate C9S [22, 49].

3.4 Concentration and buffer exchange

UF/DF was used as a CLCT concentration step and for buffer exchange to facilitate subsequent purification by chromatography. CLCT was retained by the 30-kDa membrane as expected, with no product found in the permeate. This allowed efficient buffer exchange, a 2.6-fold concentration, and a recovery of ~ 65% at a purity of 78.4 ± 5.2% TSP (n = 3) (Fig. 4). These results were comparable to reported values for FQS also produced in plants [41]. One explanation for the observed product loss could be membrane fouling due to the high load of HCP (~ 0.1 g L^{-1}) in the extracts (Fig. 3B), causing the nonspecific binding of CLCT to the membrane surface [50]. Furthermore, the long concentration process time of up to 2 h could lead to partial CLCT protein unfolding due to the increasing heat and shear stress. A major impurity co-purifying with CLCP was a ~ 18-kDa HCP, probably the small subunit of ribulose-1,5-bisphosphate carboxylase/oxygenase (RuBisCO). This protein typically forms hexadecamers of ~ 540 kDa, but we speculate that the enzyme complex disassembled during blanching and some monomers remained in the extract. Therefore, UF/DF purification as reported for other proteins such as cyanovirin-N [50], was not possible for CLCT. A major limitation in this context was the lack of diversity in MMCO values for commercially available UF/DF membranes, which restricted the process development options in terms of CLCT retention [31]. Specifically, membranes with a MMCO of 50–80 kDa would ensure CLCT retention while allowing small HCPs to pass.

3.5 Chromatography resin screening

We evaluated seven HIC resins (Fig. 5) with a CV of 0.2 mL for their ability to bind CLCT and plant HCPs present in the UF/DF retentate. The goal was to retain CLCT under high-salt conditions (140 mS cm^{-1}) on the column to facilitate stepwise elution, as observed for Phenyl Sepharose 6 FF (LS) and Butyl Sepharose HP (Fig. 5A). Compared to Butyl Sepharose HP, Phenyl Sepharose 6 FF (LS) resulted in a 1.48-fold stronger signal in the elution fraction based on densitometric analysis. However, for most of the screened resins, intense CLCT signals were also found in the flow through (FT) fractions. For example, 90% of CLCT was lost in the FT fraction of Phenyl Sepharose 6 FF (HS), whereas 42% was lost for Octyl Sepharose

Fig. 4 Evaluation of UF/DF membranes with MMCO values of 30 kDa for the purification of CLCT. Overlay of stained gel and immunoblot of retentate and permeate samples from CLCT purification using a Sartopore Hydrosart membrane (Sartorius, Göttingen, Germany) with a MMCO value of 30 kDa. Immunoblot was probed using a mouse primary monoclonal antibody against PfCSP-TSR (Table 1) and an AP-conjugated goat anti-mouse (GAM^{AP}) secondary antibody. Marker–PageRuler pre-stained protein ladder (10–177 kDa), Hom – homogenate
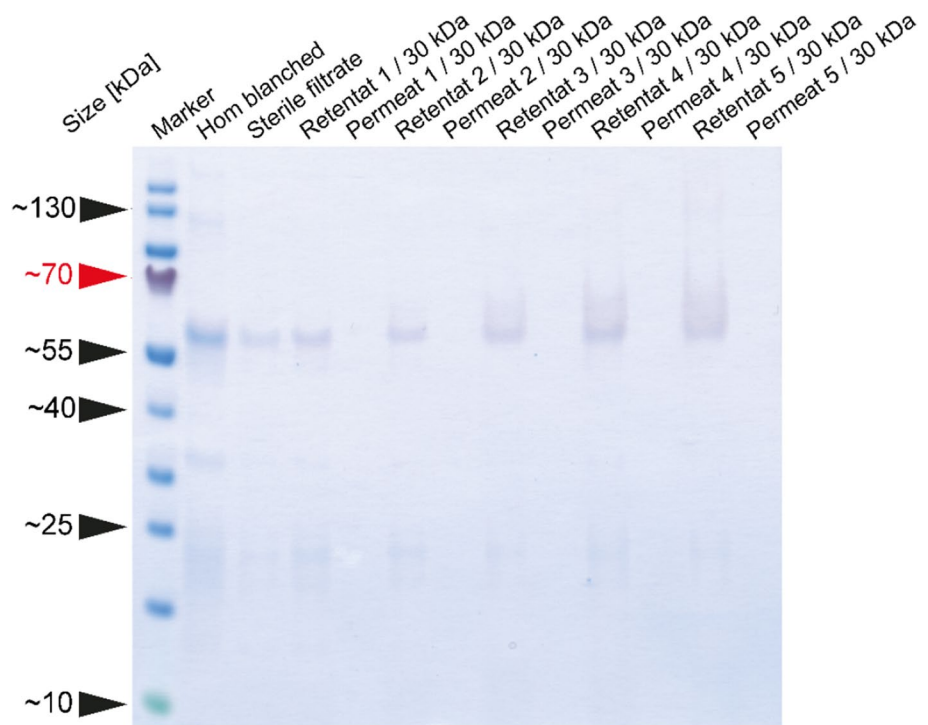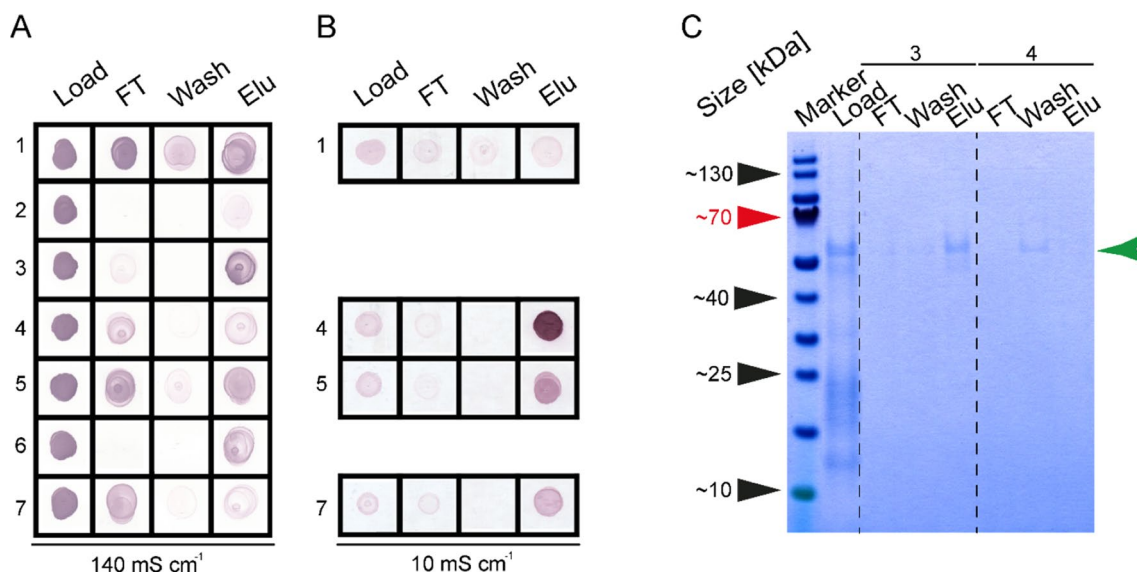
Fig. 5 High-throughput HIC resin scouting for the purification of CLCT from plant extracts. **A, B** Dot blots of HTS samples representing various HIC resins (1–7) using a high salt load at 140 mS cm^{-1} and **B** a low salt load at ~10 mS cm^{-1} for four selected resins (1, 4, 5 and 7). 1 – Phenyl Sepharose 6FF (HS), 2 – Phenyl Sepharose HP, 3 – Phenyl Sepharose 6 FF (LS), 4 – Octyl Sepharose 4 FF, 5 – Butyl Sepharose 4 FF, 6 – Butyl Sepharose HP, 7 – ButylS Sepharose, FT – flow through fraction, Elu – elution fraction. The blots were probed using a mouse primary monoclonal antibody against *Pf*CSP-TSR and an AP-conjugated goat anti-mouse (GAM^{AP}) secondary antibody (Table 1). **C** Samples of a 1.0-mL CV small-scale HIC purification of CLCT (green arrow) analyzed by LDS-PAGE and staining with Coomassie Brilliant Blue. The image contrast was increased to improve legibility using photopea (https://www.photopea.com/) by reducing the offset from 0.0 to -0.3 and increasing the gamma correction from 0.0 to 0.5. The original and unmodified image is shown in Figure S2. Resins are identified using the same numbers as in panels A and B. Marker – PageRuler pre-stained protein ladder (10–177 kDa), Load – concentrated CLCT at a conductivity of ~140 mS cm^{-1} (in **A** and **C**) or at a conductivity of ~10 mS cm^{-1} (in **B**), *Elu* Elution, *FT* Flow through

4 FF, 67% for Butyl Sepharose 4 FF and 71% for Butyl-S Sepharose (Fig. 5A). Therefore, the purification of CLCT in flow-through mode was tested for Octyl Sepharose 4 FF, Butyl Sepharose 4 FF and Butyl S Sepharose using plant extracts at a conductivity of 10 mS cm^{-1} (Fig. 5B). Surprisingly, CLCT still bound to the resins under these conditions.

3.6 Chromatography scale-up and optimization

Repeating the low-salt binding experiments at the 1.0-mL CV scale, 38% of CLCT was eluted from the Phenyl Sepharose 6 FF (LS) resin whereas in the case of Octyl Sepharose ~60% of the CLCT appeared in the flow through and wash fractions, with no major product band in the elution fraction (Fig. 5C). Because Phenyl Sepharose 6 FF (LS) achieved the most consistent binding of CLCT at the 0.2-mL and 1.0-mL CV scales, i.e. strong binding of CLCT at high and low salt loading conditions (Fig. 5A and C respectively; resin #3), this resin was used for further development of the purification step.

In a DoE approach applied to the load and elution buffers using 1.0 mL Phenyl Sepharose 6 FF (LS) columns, the load conductivities were varied between 10 and 140 mS cm^{-1}, the load and elution pH were varied between 6.0 and 8.0, and the elution buffer conductivities were varied between 0 and 10 mS cm^{-1}. The resulting model was of high quality with R^2 values > 0.89 (Table S2) [51]. As expected, the purification of CLCT was most efficient at high loading conductivities and low elution buffer conductivities in the range 0–2 mS cm^{-1} (Fig. 6A), reaching a purity of up to 83% of TSP and 41% recovery in a single chromatography step. The latter was comparable to recoveries reported for other one-step HIC purifications [52, 53], and might be increased in the future by using an even higher loading conductivity. Interestingly, the pH had no significant effect on the purity in the range we investigated (Fig. 6B), in good agreement with proteins similar to CLCT [41, 54] and protein separation by HIC in general [55, 56]. This allows the use of neutral pH, which can stabilize target proteins sensitive to extreme pH [54]. CLCT binding was also possible at low conductivities such as 10 mS cm^{-1} and elution was even possible using pure water (Fig. 6C). These results correspond to the outcomes of the initial HTS experiments and confirmed the strong hydrophobic interaction between CLCT and the HIC resins (Fig. 5).
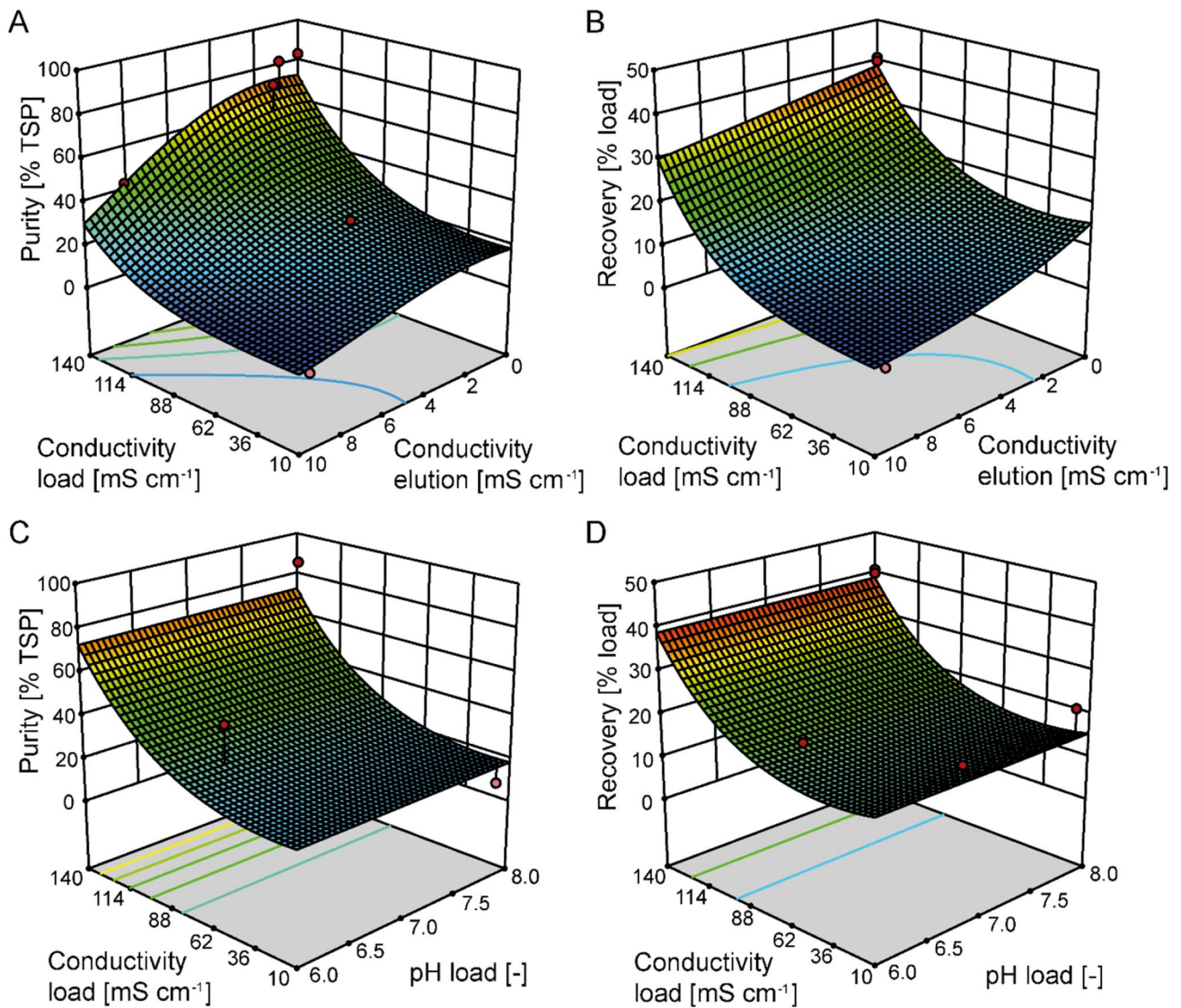
Fig. 6 Response surfaces illustrating the effect of load/elution buffer pH and conductivity on the purity (**A** and **C**) and recovery (**B** and **D**) of CLCT in HIC elution fractions. CLCT purity was based on the analysis of stained gels following LDS-PAGE. The highest purity was achieved at high load conductivities and low elution conductivities whereas the pH value had no relevant effect (**B**). CLCT yields were calculated based on LDS-PAGE and immunoblot results. **C** CLCT recoveries were highest at high load conductivities and low elution conductivities whereas the pH had no relevant effect on elution behavior (**D**). Red dots indicate experimental runs. Model runs below the response surface are not visible from the perspective shown. Correlation factors of the model are shown in Table S2 and numerical optimization in Table S3. *TSP* Total soluble protein

3.7 Stability of purified CLCT

Interestingly, we observed that substantial fractions of CLCT were lost when samples were stored even for only a short time. For example, the CLCT recovery was ~20% in homogenate samples incubated at 4 °C for 96 h (Fig. 7). Binding to the container surfaces or proteolytic degradation might explain this observation, so we analyzed CLCT concentrations over 96 h when stored in polypropylene or glass reaction tubes, the latter of which typically exhibit low protein binding due to the hydrophilic surface. Interestingly, no significant difference (t-test, p value = 0.867) between samples stored in polypropylene or glass containers was observed (Fig. 7A).

Whereas CLCT was significantly more stable in elution fractions compared to the homogenate (ttest, p = 0.033), CLCT yields in the former still decreased linearly by 12 ± 2% (± SD, n = 2) after 24 h and 49 ± 5% (± SD, n = 2) after 96 h (Fig. 7B). This indicated a depletion of impurities such as endogenous plant proteases that could be responsible for
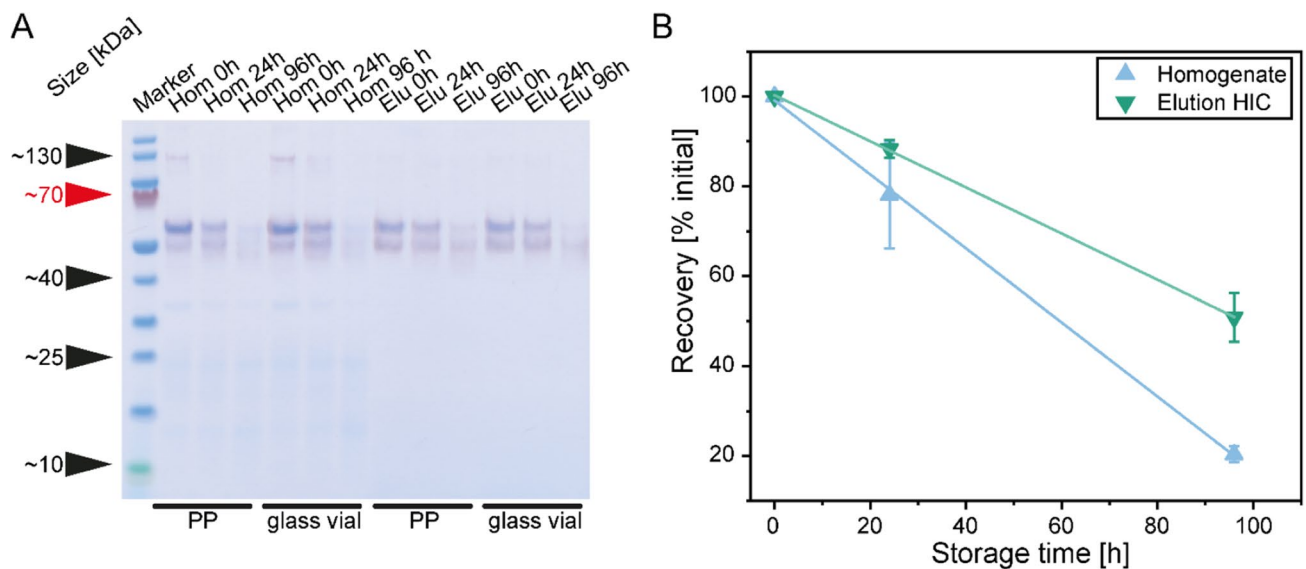
Fig. 7 Stability of purified CLCT produced in plants. **A** Overlay of stained gel and immunoblot of homogenate (Hom) and elution (Elu) samples after 0, 24 and 96 h storage at 4 °C in either polypropylene (PP) containers or glass vials. Marker – PageRuler prestained protein ladder (10–177 kDa). Immunoblots were probed using a mouse primary monoclonal antibody against *Pf*CSP-TSR and an AP-conjugated goat anti-mouse (GAM[AP]) secondary antibody (Table 1). **B** Stability of purified CLCT based on immunoblot data. Linear fitting with R^2 values > 0.99 for the recovery of CLCT in the homogenate (slope -0.82 ± 0.02) and HIC elution (slope -0.51 ± 0.01). HIC – hydrophobic interaction chromatography

proteolysis of the target protein during purification [57]. Accordingly, even after blanching, active proteases can be present in plant extracts and only highly-purified CLCT might provide an acceptable stability. The linearity of CLCT loss over time in both sample types suggests a saturated enzymatic reaction, with higher protease concentrations in the homogenate causing faster degradation compared to the purified CLCT in the HIC eluate. Overall, HIC purification was sufficient to provide CLCT sample material for initial activity testing, but size exclusion chromatography may be necessary as a further polishing step in the future.

4 Conclusion

The malaria vaccine candidate CLCT was produced in *N. benthamiana* by transient expression, with accumulation levels of 118.8 ± 20.4 mg kg^{-1}. Blanching of infiltrated plants facilitated not only the precipitation of > 90% of TSP, but also increased the stability of CLCT in the crude plant extract as previously shown for a similar malaria vaccine candidate. HIC was used to purify the CLCT protein and only one further polishing step might be required to achieve the purity levels required for biopharmaceutical proteins as defined by the regulatory authorities. The low overall process yield of ~ 9.8% (~ 11.7 mg kg^{-1}) mainly resulted from CLCT losses during depth filtration and UF/DF. Further improvements in the purification process and an additional polishing step could fix the stability problems of CLCT and could achieve purities > 95% TSP.

Given that manufacturing costs for plant-derived biopharmaceutical proteins are ~€250 per kg biomass in VFUs [30, 35], the production of the main vaccine component before formulation (e.g. without adjuvants etc.) would cost ~ 21,000 € g^{-1}. About 2.34 g CLCT could be produced per month based on a production capacity of 200 kg plant biomass per month [22, 30, 41]. Recent reports indicate that ~ 30 µg vaccine protein is required for one dose for comparable malaria vaccine candidates such as FQS or the CSP-containing malaria vaccine candidate RTS/S [7, 58, 59]. Assuming a similar dose for CLCT and combined with the anticipated overall process yield after process optimization, ~ 78,000 vaccine doses could be produced per month and almost one million individuals could be supplied with the malaria vaccine per year for the given scenario using a small 200-kg pilot scale production site. The cost of the antigen component (i.e. the recombinant CLCT) would be ~ 0.63 € per dose in such a scenario, but additional cost will emerge for formulation, packing (e.g. syringes) and distribution. There are ~ 60 million births per year (2007 data) in regions with endemic *P. falciparum* malaria [60], and vaccination requires at least one booster dose to achieve an acceptable protection level of > 75%, so

~ 24 tonnes of biomass would be required to produce sufficient amounts of CLCT vaccine. Further DSP optimization could reduce that amount, and cultivation in VFUs could facilitate a continuous supply [29, 61, 62]. With these improvements, plant-made CLCT would help to reduce malaria transmission in low-and-middle-income countries. Further investigation is therefore necessary to improve the DSP efficiency for this vaccine candidate. In addition, characterization, e.g. in terms of aggregation, as well as activity testing by in vitro and in vivo efficacy assays should follow to assess the plant-made vaccine candidate in more detail as described for similar proteins [23]. In this context, the effect of any aberrant glycosylation that could unintentionally shield relevant epitopes on the vaccine candidate can be assessed. For example, adverse glycosylation sites can be removed by mutation and plant lines devoid of plant-specific glycosyltransferases or those expressing, for example, human glycosyltransferases can be used if necessary [63].

Data availability The data that support the findings of this study are available from the corresponding author upon reasonable request.

Code availability Not applicable.

Declarations

Ethics approval and consent to participate Not applicable.

Consent for publication All authors have seen a draft version of the manuscript and concur with its submission to the journal.

Competing interests The authors have no competing interest to declare.

References

1. WHO. Malaria fact sheet who.int. Geneva: WHO; 2017.
2. Farrow RE, Green J, Katsimitsoulia Z, Taylor WR. The mechanism of erythrocyte invasion by the malarial parasite, *Plasmodium falciparum*. Semin Cell Dev Biol. 2011;22(9):953.
3. Wassmer SC, Taylor TE, Smith JD. Investigating the pathogenesis of severe malaria: a Multidisciplinary and Cross-Geographical Approach. Am J Trop Med Hyg. 2015;93:42–56.
4. Talapko J, et al. Malaria: the past and the present. Microorganisms. 2019;7(6):179.
5. White NJ, et al. Malar Lancet. 2014;383(9918):723–35.
6. WHO. World malaria report who.int. Geneva: WHO; 2016.
7. Boes A, Spiegel, Holger V, Nadja. Analysis of a multi-component multi-stage Malaria Vaccine candidate—tackling the cocktail challenge. Public Libr Sci One. 2015;10(7):e0131456.
8. Amador R, Moreno A, Falla JC. Safety and immunogenicity of the synthetic malaria vaccine SPf66 in a large field trial. J Infect Dis. 1992;166(1):139–44.
9. Seder RA, Chang LJ, Enama ME. Protection against malaria by intravenous immunization with a nonreplicating sporozoite vaccine. Science. 2013;341(6152):1359–65.
10. Doolan DL, Hoffman SL. DNA-based vaccines against malaria: status and promise of the multi-stage malaria DNA vaccine operation. Int J Parasitol. 2001;31(8):753–62.
11. Stoute JA, et al. A preliminary evaluation of a recombinant circumsporozoite protein vaccine against *Plasmodium falciparum* malaria. RTS,S malaria vaccine evaluation group. N Engl J Med. 1997;336(2):86–91.

12. Schwartz L, Brown GV, Genton, Blaise, Moorthy, Vasee S. A review of malaria vaccine clinical projects based on the WHO rainbow table. Malar J. 2012;11(1):11.

13. Srinivasan PE, Diouf E. Immunization with a functional protein complex required for erythrocyte invasion protects against lethal malaria. Proc Natl Acad Sci USA. 2014;111(28):10311–6.

14. Olotu A, Fegan G. Four-year efficacy of RTS,S/AS01E and its interaction with malaria exposure. N Engl J Med. 2013;368(12):1111–20.

15. Foquet L, Hermsen CC, Meuleman P, Leroux-Roels G. Vaccine-induced monoclonal antibodies targeting circumsporozoite protein prevent Plasmodium falciparum infection. J Clin Invest. 2014;124(1):140–4.

16. Datoo MS, et al. Efficacy and immunogenicity of R21/Matrix-M vaccine against clinical malaria after 2 years' follow-up in children in burkina faso: a phase 1/2b randomised controlled trial. Lancet Infect Dis. 2022;22(12):1728–36.

17. Boes A, Spiegel H, Edgue G, Kapelski S, Scheuermayer M, Fendel R, Fischer R. Detailed functional characterization of glycosylated and nonglycosylated variants of malaria vaccine candidate PfAMA1 produced in Nicotiana benthamiana and analysis of growth inhibitory responses in rabbits. Plant Biotechnol J. 2015;13(2):222–34.

18. Morahan BJ, Wang L, Coppel RL. No TRAP, no invasion. Trends Parasitol. 2009;25(2):77–84.

19. Voepel NB, Edgue A, Beiss G, Fischer V. Malaria vaccine candidate antigen targeting the pre-erythrocytic stage of Plasmodium falciparum produced at high level in plants. Biotechnol J. 2014;9(11):1435–45.

20. Zhao J, Bhanot Purnima Hu, Junjie W, Qian. A comprehensive analysis of Plasmodium circumsporozoite protein binding to hepatocytes. Public Library Sci One. 2016;11:e0161607. https://doi.org/10.1371/journal.pone.0161607.

21. Bergmann-Leitner E, Ryan Mease M, et al. Immunization with pre-erythrocytic antigen CelTOS from Plasmodium falciparum elicits cross-species protection against heterologous challenge with Plasmodium berghei. Plus One. 2010;5:e12294.

22. Menzel S, et al. Optimized blanching reduces the host cell protein content and substantially enhances the recovery and stability of two plant-derived malaria vaccine candidates. Front Plant Sci. 2016;7(159):1–7.

23. Boes A, et al. Analysis of a multi-component multi-stage Malaria Vaccine candidate–tackling the cocktail challenge. PLoS ONE. 2015;10(7):e0131456.

24. Beiss V, Spiegel Holger. Heat-precipitation allows the efficient purification of a functional plant-derived malaria transmission-blocking vaccine candidate fusion protein: heat-precipitation allows the efficient purification. Biotechnol Bioeng. 2015;112:1297.

25. Bowman S, et al. The complete nucleotide sequence of chromosome 3 of Plasmodium falciparum. Nature. 1999;400(6744):532–8.

26. Knödler M, Buyel JF. Plant-made immunotoxin building blocks: a roadmap for producing therapeutic antibody-toxin fusions. Biotechnol Adv. 2020;47:107683.

27. Opdensteinen P, Meyer S, Buyel JF. Nicotiana spp. for the expression and purification of functional IgG3 antibodies directed against the Staphylococcus aureus alpha toxin. Front Chem Eng. 2021; 3(50).

28. Knödler M, et al. Seasonal weather changes affect the yield and quality of recombinant proteins produced in transgenic tobacco plants in a greenhouse setting. Front Plant Sci. 2019;10:1245.

29. Huebbers JW, Buyel JF. On the verge of the market – plant factories for the automated and standardized production of biopharmaceuticals. Biotechnol Adv. 2021;46:107681.

30. Buyel JF, Fischer R. Very-large-scale production of antibodies in plants: the biologization of manufacturing. Biotechnol Adv. 2017;35(4):458–65.

31. Buyel JF. Extraction and downstream processing of plant-derived recombinant proteins. Biotechnol Adv. 2015;33(6):902–13.

32. Buyel JF, Gruchow HM, Boes A, Fischer R. Rational design of a host cell protein heat precipitation step simplifies the subsequent purification of recombinant proteins from tobacco. Biochem Eng J. 2014;88:162–70.

33. Olsnes S, Haylett T, Refsnes K. Purification and characterization of the highly toxic lectin modeccin. J Biol Chem. 1978;253(14):5069–73.

34. Houdelet M, Holland, Tanja B, Felix J. Animal component-free agrobacterium tumefaciens cultivation media for better GMP-compliance increases biomass yield and pharmaceutical protein expression in Nicotiana benthamiana. Biotechnol J. 2017;12(4):1600721-n/a.

35. Knödler M, et al. Simple plant-based production and purification of the assembled human ferritin heavy chain as a nanocarrier for tumor-targeted drug delivery and bioimaging in cancer therapy. Biotechnol Bioeng. 2023;120(4):1038–54.

36. Knödler M. Development and plant-based expression of recombinant immunotoxins for the targeted treatment of myelomonocytic leukemia. RWTH Aachen University: Veröffentlicht auf dem Publikationsserver der RWTH Aachen University; in 2023. p. 155.

37. Simmons CW, VanderGheynst JS, Upadhyaya SK. A model of Agrobacterium tumefaciens vacuum infiltration into harvested leaf tissue and subsequent in planta transgene transient expression. Biotechnol Bioeng. 2009;102(3):965–70.

38. Buyel JF, Gruchow M. Fischer, rainer, depth filters containing diatomite achieve more efficient particle retention than filters solely containing cellulose fibers. Front Plant Sci. 2015;6(1134):e51216.

39. Bradford MM. A rapid and sensitive method for the quantitation of microgram quantities of protein utilizing the principle of protein-dye binding. Anal Biochem. 1976;72(1):248–54.

40. Buyel JF, Fischer R. Characterization of complex systems using the design of experiments approach: transient protein expression in tobacco as a case study. J Vis Exp. 2014;83:51216.

41. Menzel S, Holland T, Boes A, Spiegel H, Fischer R, Buyel JF. Downstream processing of a plant-derived malaria transmission-blocking vaccine candidate. Protein Exp Purif. 2018;152:122–30.

42. Gengenbach BB, et al. Comparison of microbial and transient expression (tobacco plants and plant-cell packs) for the production and purification of the anti-cancer mistletoe lectin viscumin. Biotechnol Bioeng. 2019;116(9):2236–49.

43. Sack M, Paetz A, Kunert R, Bomble M, Hesse F, Stiegler G, Fischer R. Functional analysis of the broadly neutralizing human anti-HIV-1 antibody 2F5 produced in transgenic BY-2 suspension cultures. FASEB J. 2007;21(8):1655–64.

44. Floss DMS, Stadlmann M. Biochemical and functional characterization of anti-HIV antibody-ELP fusion proteins from transgenic plants. Plant Biotechnol J. 2008;6(4):379–91.

45. Shamloul M, Trusa J, Mett V, Yusibov V. Optimization and utilization of agrobacterium-mediated transient protein production in Nicotiana. J Vis Exp. 2014;86:51204.

46. Buyel F, Hubbuch J, Fischer J. Rainer, comparison of tobacco host cell protein removal methods by blanching intact plants or by heat treatment of extracts. J Vis Exp. 2016;2016:54343.

47. Yigzaw Y, et al. Exploitation of the adsorptive properties of depth filters for host cell protein removal during monoclonal antibody puri-fication. Biotechnol Prog. 2006;22(1):288–96.

48. Buyel JF, Fischer POR. Cellulose-based filter aids increase the capacity of depth filters during the downstream processing of plant-derived biopharmaceutical proteins. Biotechnol J. 2015;10(4):584–91.

49. Menzel S. Downstream processing of malaria vaccine candidates and modeling of chromatography PhD Thesis RWTH Aachen University, 2018.

50. Opdensteinen P, et al. A combined ultrafiltration/diafiltration step facilitates the purification of cyanovirin-N from transgenic tobacco extracts. Front Bioeng Biotechnol. 2019;6:206.

51. Kleppmann W. Versuchsplanung - produkte und prozesse optimieren Hanser, 2018(8th edition).

52. Kocabas A. One-step purification and characterization of a low molecular weight xylanase from *Aspergillus terreus* NRRL 1960. J Appl Biol Sci, 2011. Vol. 5.

53. Sewekow E, et al. Isolation of soybean protein P34 from oil bodies using hydrophobic interaction chromatography. BMC Biotechnol. 2008;8(1):27.

54. Baumann P, Baumgartner K, Hubbuch J. Influence of binding pH and protein solubility on the dynamic binding capacity in hydrophobic interaction chromatography. J Chromatogr A. 2015;1396:77–85.

55. Hjertén S, Yao K, Eriksson K-O, Johansson B. Gradient and isocratic high performance hydrophobic interaction chromatography of proteins on agarose columns. J Chromatog. 1986;359:99–109.

56. AmershamBiotech. Hydrophobic Interaction Chromatography: principles and methods. Amersham Biotechnol, 2000. 18–020.

57. Palma JM, Sandalio LM, del Río LA. Plant proteases, protein degradation, and oxidative stress: role of peroxisomes. Plant Physiol Biochem. 2002;40(6):521–30.

58. Moorthy VS, Ballou WR. Immunological mechanisms underlying protection mediated by RTS,S: a review of the available data. Malar J. 2009;8(1):312.

59. Takeyama N, Kiyono H, Yuki Y. Plant-based vaccines for animals and humans: recent advances in technology and clinical trials. Volume 3. Ther Adv Vaccines Immunother; 2015.

60. Dellicour S, et al. Quantifying the number of pregnancies at risk of Malaria in 2007: a demographic study. PLoS Med. 2010;7(1):e1000221.

61. Schillberg S, Finnern R. Plant molecular farming for the production of valuable proteins - critical evaluation of achievements and future challenges. J Plant Physiol. 2021;258:153359.

62. Chung YH, et al. Integrating plant molecular farming and materials research for next-generation vaccines. Nat Rev Mater. 2021;7:372.

63. Dicker M, et al. Transient glyco-engineering to produce recombinant IgA1 with defined N- and O-Glycans in plants. Front Plant Sci. 2016;7:18.

64. Myers RHaM. D. C., Response surface methodology: process and product optimization using designed experiment. John Wiley & Sons. Inc.; 1995.